Annals of Biomedical Engineering, Vol. 31, pp. 294–309, 2003
Printed in the USA. All rights reserved.

0090-6964/2003/31(3)/294/16/$20.00

Analysis of Nitric Oxide Consumption by Erythrocytes in Blood Vessels using a Distributed Multicellular Model

NAEL H. EL-FARRA, PANAGIOTIS D. CHRISTOFIDES, and JAMES C. LIAO

Department of Chemical Engineering, University of California, Los Angeles, CA

(Received 18 December 2001; accepted 12 December 2002)

Abstract—Multiple sets of experimental data have shown that the red blood cell (RBC) consumes nitric oxide (NO) about 600–1000-fold slower than the equivalent concentration of cell-free hemoglobin (Hb). Diffusion barriers of various sources have been suggested to explain this observation. In this work, a multicellular, spatially distributed, two-dimensional model, that describes the production, transport, and consumption of NO in blood vessels and the surrounding tissue, is developed. The model is used to assess the relative significance of NO transport barriers that reduce the rate of NO consumption in the blood. Unlike previous models of this system, the model developed here accounts explicitly for the presence of, and interactions among, a population of RBCs inside the lumen of the blood vessel and is, therefore, better suited to analyze, quantitatively, the contribution of each transport barrier as NO diffuses from its site of synthesis to the interior of the RBCs where it interacts with Hb. The model, which uses experimentally derived parameters, shows that extracellular unstirred boundary layer diffusion alone cannot account for the reduced NO consumption by RBC compared to an equivalent concentration of cell-free Hb. Since this result is reached using a two-dimensional representation of the RBCs, which overestimates the importance of the boundary layer diffusion resistance, it would be expected that in the real three-dimensional case, diffusion through the extracellular boundary layer would contribute even less to the overall mass transfer resistance. Consistent with recent experimental findings, the results of our model suggest that, under physiological conditions, transmembrane (membrane and its associated cytoskeleton layer) diffusion limitations in RBCs represent a key source of resistance for NO uptake by RBCs. *© 2003 Biomedical Engineering Society.* [DOI: 10.1114/1.1553454]

Keywords—Nitric oxide, Diffusion reaction, Red blood cells, Mass transfer resistance, Computational modeling.

INTRODUCTION

The problem of computational modeling of nitric oxide (NO) transport–reaction processes in blood vessels has been the subject of significant research over the past decade. Interest in this problem has been motivated by the physiological significance of NO itself as a versatile reactive free radical that participates in a diverse array of vital biological functions in humans and animals such as vascular regulation, inhibition of platelet aggregation, and immunological responses (see Ref. 9 for details and references). Enhanced understanding of the key mechanisms for NO transport and consumption, through computational modeling coupled with experiments, has crucial implications for the development of practical technologies (e.g., artificial blood substitutes) that can be used to treat diseases attributed to imbalances in NO bioavailability.

The transport of NO from its site of synthesis to its target is a complex process that is under intensive investigation. In order to exercise its vasoregulatory effect in the microcirculation, NO must diffuse from the endothelium lining blood vessel walls to the external surrounding tissue (vascular smooth muscle) where it activates its primary target, soluble guanylate cyclase. Due to its reactivity, however, NO may be consumed and degraded by numerous reactions before it reaches its target. In particular, NO diffuses into the lumen of the blood vessel where it reacts at very high rates with Hb in red blood cells (RBCs).[4,5,7] The extremely fast kinetics of this reaction, however, suggest that most of the NO produced in the endothelium would be consumed in the blood, severely limiting NO bio-availability in the vascular smooth muscle. Indeed, mathematical modeling based on diffusion theory and *in vitro* measurements of kinetic constants have confirmed that Hb could effectively scavenge endothelial produced NO and mitigate its effect.[11,28,29] Given that small amounts (μM) of free Hb can abolish NO-mediated vasodilation *in vitro*,[12,18] NO consumption by RBCs must be much slower than originally expected. Carlsen and Comroe[3] were the first to report that the reaction between NO and Hb in intact human RBCs was slower than others measured in Hb solutions. They speculated that membrane diffusion resistance might account for their experimental results, although they could not rule out the possibility that the reaction rate might be slower inside red blood cells with more concentrated Hb than others measured with more

Address correspondence to James C. Liao at Department of Chemical Engineering, University of California, Los Angeles, CA 90095-1592. Electronic mail: liaoj@ucla.edu

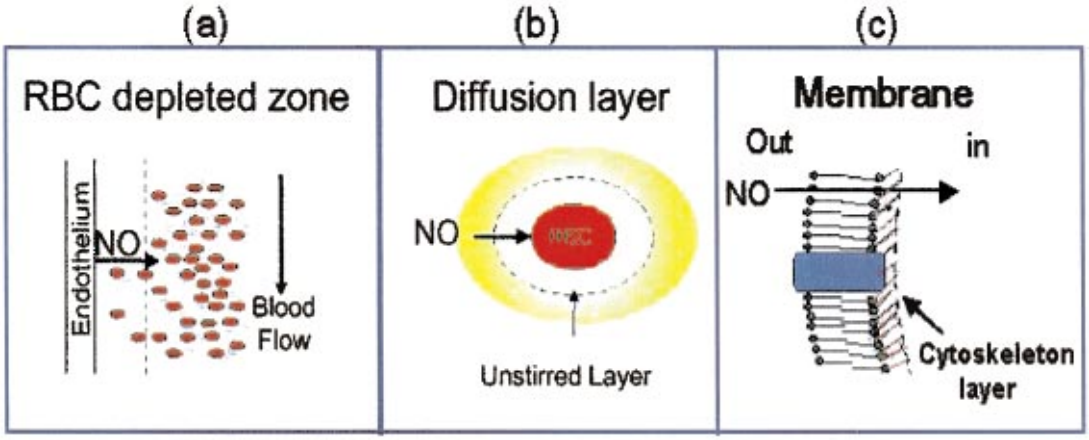

FIGURE 1. Potential barriers for NO transport as it diffuses from the endothelium across a cell-depleted zone (a), into the extracellular space surrounding the RBCs (b), and across the RBC membrane (c) before it is consumed by Hb in the cytosol.

dilute cell-free Hb solutions. This apparent discrepancy, therefore, has been known for over four decades, and has generated recent interest now that the biological significance of NO is known.

The low rate of NO uptake has been attributed to hindrances to NO transport caused by diffusion through: (i) RBC-depleted region that intravascular flow creates near the vessel wall,[2,12,28] (ii) the undisturbed (boundary) layer around the RBC,[13,19] and (iii) a RBC-membrane associated barrier[8,26] (see Fig. 1). The diffusion inside the RBC has been shown to be nonlimiting.[8] While the three barriers may contribute, the relative importance of each barrier has been difficult to assess. This assessment can be made, however, through detailed mathematical modeling of NO reaction–diffusion processes in blood vessels. Previous modeling efforts were reviewed and summarized in Ref. 1. In particular, a mathematical formulation[28] that accounts for the geometry of NO production and consumption regions was developed to determine factors that affect the NO concentration and the effective diffusion distance, especially in the microcirculation. In this model,[28] the blood was treated as a continuum, i.e., a homogeneous medium where NO consumption by Hb takes place uniformly throughout. In addition to these efforts, the modeling of NO uptake by a single red blood cell was considered in Ref. 27. The model in this case takes into account the resistances of the diffusional layer around the RBC, the membrane, and the intracellular interactions between NO and Hb. By applying the model in Ref. 27 to experimental data, the authors obtained estimates of the membrane permeability.

While the previous works have made significant contributions to the modeling and analysis of NO transport and reaction, the particulate nature of the blood, namely, the presence of, and interactions among, a population of RBCs inside the lumen of the blood vessel (as opposed to a homogeneous medium or just a single RBC where NO reacts with Hb), has not been considered in any of the existing models so far, thus limiting their capability to capture or quantify the full host of transport barriers that reduce NO uptake. The particulate nature contributes to the reduction of NO uptake in the blood by diminishing the actual exposure of NO to Hb further, compared to that predicted from the continuum model, and introduces additional diffusional barriers in the extracellular spaces between cells in the population. On the other hand, single cell models cannot account for intercellular diffusion realistically. Motivated by these considerations, we develop in this study a detailed two-dimensional, multicellular model for NO transport, based on diffusion–reaction principles, that explicitly takes into account the presence of, and interactions among, a population of red blood cells inside the blood vessel. The model describes the production, diffusion, and consumption of NO in different regions, including the vascular smooth muscle surrounding the blood vessel, the vessel wall, a cell-free zone inside the lumen and near the vessel wall, the extracellular space between the population of RBCs in the vessel lumen, the membrane surrounding each cell, and, finally, the intracellular space inside the RBCs. The model equations consist of several sets of partial differential equations (PDEs) that describe the production, diffusion, and consumption of NO in each of these regions. The equations are coupled through the boundary conditions that govern the flux and concentration of NO at the interfaces between the different compartments. The parameters for the model are obtained from experimental data reported in the literature and the entire set of PDEs is solved for the NO concentration profile using efficient finite-element algorithms. It should be emphasized that our goal here is not to predict

the actual concentration of NO in tissue. Rather, we are interested in assessing the relative significance of each transport barrier using a more realistic model for NO transport that considers the multicellular nature of the problem and is, therefore, better suited to quantify the contribution of each barrier to the overall resistance for NO uptake in the blood.

We compare four scenarios. In the first scenario, the blood is treated as a homogenous Hb solution without RBCs. In the second scenario, the blood is modeled as a random suspension of RBCs with no transmembrane diffusion barrier. In the third scenario, a low transmembrane NO permeability is used instead of the high transmembrane permeability used in scenario 2. Finally, in the fourth scenario, a RBC-free zone near the vessel wall is added due to blood flow. NO concentration profiles computed in scenarios 2–4 are compared with the profiles obtained from scenario 1 for various values of k_{Hb}, the rate constant of the NO reaction with oxygenated Hb. This comparison allows assessment of the contribution from each diffusion barrier (inter-RBC diffusion, transmembrane diffusion, and RBC-free zone) in terms of fold reduction in k_{Hb} compared to its equivalent homogenous Hb solution. Results show that the extracellular diffusion barrier caused by the unstirred layer is insufficient to explain the 1000-fold reduction in NO consumption rate by RBCs under physiological hematocrits. Because of its two-dimensional representation of the RBCs, the model underestimates the diffusion rate across the extracellular boundary layer and, therefore, overestimates the boundary layer diffusion resistance. However, even under this conservative estimation, we found that the boundary layer resistance was insignificant under physiological hematocrits. We would expect that in the real RBC, where surface/volume ratio is significantly larger than what the model assumes, diffusion through the extracellular boundary layer would even be more efficient and thus contributes less to the overall mass transfer resistance. Furthermore, the effect of membrane diffusion barrier (including the cytoskeleton layer) can only be seen under high (physiological) hematocrits. These results explain in part the discrepancy between different groups.[8,13,26]

MATHEMATICAL MODELING OF NO TRANSPORT

Modeling Assumptions

To provide a detailed model that captures the main features of NO transport in blood vessels and the surrounding tissue, we divide the system into three major compartments: the abluminal region, the endothelium, and the lumen. The lumen is further divided into a cell-free zone, extracellular spaces between the cell population in the vessel, the membrane surrounding each cell, and, finally, the intracellular spaces [see Fig. 2(a)]. The system was modeled using two-dimensional polar coordinates. To keep the model realistic, yet computationally tractable, we make the following assumptions:

(1) The axial NO gradient along the vessel is small compared with the length of the region producing NO, so NO transport by convection can be neglected.
(2) The NO transport–reaction process is analyzed at steady state. This assumption is motivated by the large difference in time scales between the diffusion/reaction (on the order of 10 ms) and NO production. Therefore, transients in the NO gradient die out quickly.[27]
(3) Since NO is present in trace quantities, the diffusion coefficient is taken to be independent of concentration.
(4) The diffusion of NO is isotropic and the diffusion coefficient in a given region is the same in all directions.
(5) The main NO reaction in the blood is that with Hb, and is assumed to be pseudo-first-order in NO concentration. NO consumption in tissue is primarily through reaction with oxygen and is taken to be second order in NO concentration, with an empirically determined rate constant that sums the contribution of various NO decomposition mechanisms and reactions with other species in tissue.[29]
(6) The rate of NO production in the endothelium is estimated from the data of Malinski *et al.*[15,29] obtained by stimulating endothelial cells for NO production.

Governing Equations

The concentration of a diffusing reacting substance, such as NO, is described by the species mass balance. For NO, this balance, in its general form, can be written as

$$\frac{\partial C_{\mathrm{NO}}}{\partial t} = D_{\mathrm{NO}} \nabla^2 C_{\mathrm{NO}} - \nabla C_{\mathrm{NO}} \cdot v + R_{\mathrm{NO}}, \qquad (1)$$

where ∇ is the vector gradient operator, ∇^2 is the Laplacian operator, C_{NO} is the concentration of NO, D_{NO} is the diffusion coefficient, and R_{NO} is the rate at which NO is produced or consumed by reaction. Two processes are involved in the transport of NO: the first term on the right-hand side represents the diffusion of NO; the second represents the transport of NO by a molar-averaged velocity. From assumptions (1) and (2), we have that $\nabla C_{\mathrm{NO}} \cdot v = 0$ and $\partial C_{\mathrm{NO}} / \partial t = 0$, respectively. The system can, therefore, be treated as a two-dimensional problem, with NO concentration varying only in the radial (r) and azimuthal (θ) directions. The azimuthal variation of NO

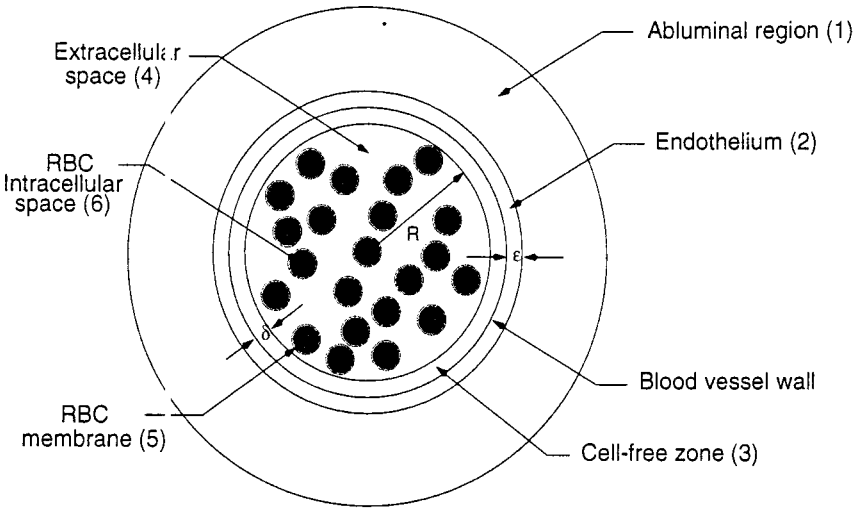

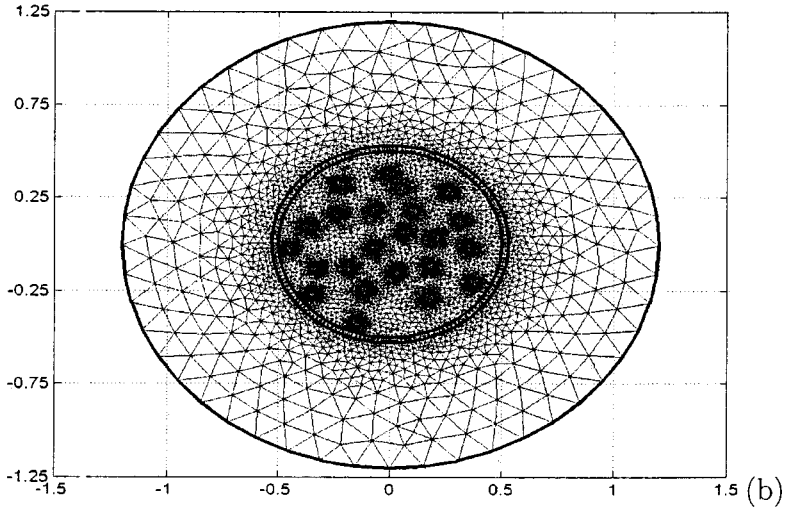

FIGURE 2. (a) Geometry of the blood vessel showing the various compartments of the model and a distribution of RBCs. (b) Example of the finite-element mesh used to discretize the spatial domain in the luminal, abluminal, and endothelial regions of the blood vessel. Finer mesh is used closer to the interfaces.

concentration arises from nonuniform consumption of NO inside the vessel due to a nonuniform (random) distribution of cells. The balance between NO diffusion and reaction in all compartments can be written for polar coordinates as

$$D_{\mathrm{NO}}\left[\frac{1}{r}\frac{\partial}{\partial r}\left(r\frac{\partial C_{\mathrm{NO}}}{\partial r}\right)+\frac{1}{r^2}\frac{\partial^2 C_{\mathrm{NO}}}{\partial \theta^2}\right]+R_{\mathrm{NO}}=0. \qquad (2)$$

Equation (2) is used for all compartments, although the value of D_{NO} may differ depending on the intrinsic transport resistance in each region. Also, the expression for R_{NO} may differ in each region depending on whether NO is being produced or consumed and depending on the rate laws of the chemical reactions taking place in each region.

In the abluminal region, NO is assumed to be consumed by a second-order reaction,[28] so R_{NO} takes the form

$$R_{\mathrm{NO}}=-k_{ab}C_{\mathrm{NO}}^2, \qquad (3)$$

where k_{ab} is an overall reaction rate constant that accounts for the contribution of various NO decomposition mechanisms and reactions with other species in the smooth muscle tissue. The value of k_{ab} was estimated by fitting the data of Malinski *et al.*[15] to a one-dimensional homogeneous model, developed in Ref. 29, based on oblate spherical coordinates.

In the endothelium, NO is also consumed by the above second-order reaction but, in addition, it is produced by an enzyme that is partially bound to the mem-

TABLE 1. Model parameters.

Parameter Definition	Symbol	Value	Unit	Reference
Extracellular NO diffusion coefficient	D_{ext}	3300	$\mu m^{2\,s^{-1}}$	15,29
Intracellular NO diffusion coefficient	D_{int}	880	$\mu m^2\,s^{-1}$	27
RBC membrane permeability	$P_{RBC,est}$	450	$\mu m\,s^{-1}$	27
Lipid membrane permeability	P_{lipid}	9×10^5	$\mu m\,s^{-1}$	27
Abluminal NO reaction rate coefficient	k_{ab}	0.05	$\mu m^{-1}\,s^{-1}$	28
OxyHb-NO reaction rate coefficient	k_{Hb}	8.9×10^7	$M^{-1}\,s^{-1}$	7
Total NO production rate in endothelium	Q_{NO}	42.4	$\mu M\,s^{-1}$	15,28
Blood vessel radius	R	50	μm	28
RBC-free zone thickness	δ	2.5	μm	28
Endothelium thickness	ϵ	2.5	μm	28
Effective radius of RBC	a	3.39	μm	27
RBC membrane thickness	δ_{RBC}	0.0078	μm	27
Hb concentration in RBC	$C_{Hb,RBC}$	23	mM	27

brane of endothelial cells (constitutive NO synthase). The expression for R_{NO} in this compartment, therefore, takes the form

$$R_{NO}=-k_{ab}C_{NO}^2+Q_{NO}, \tag{4}$$

where Q_{NO} is the total NO production rate in the endothelium. The rate of NO production is computed by dividing the total molar flux of NO in the endothelium, $\dot{q}_{NO}$ (estimated from the data of Malinski *et al.*[15] to be 10.6×10^{-14} μmol/μm^2 s), by the thickness of the endothelium, ϵ, i.e., $Q_{NO}=\dot{q}_{NO}/\epsilon$ (see Table 1). The rate expression in Eq. (4) is different from the one used in Ref. 28 for the same region. In Ref. 28, the NO production term was not included in the expression for R_{NO}. Instead, NO production was accounted for in the flux boundary conditions (through surface mass balances) where NO was assumed to be produced from two singular surfaces that bound the endothelium (the endothelial/luminal and endothelial/abluminal interfaces). The net fluxes at both surfaces were assumed to be the same, with the value of each flux equaling half of $\dot{q}_{NO}$. In Eq. (4), the production of NO is assumed to take place uniformly inside the endothelium rather than at the interfaces. The validity of both approximations owes to the relatively small thickness of the endothelium compared with other spatial dimensions in the problem.

In the extracellular vascular lumen and inside the RBC membrane, NO is transported by diffusion (with a different diffusivity in each region) and R_{NO} is taken to be zero. This treatment is justified because the third-order NO reaction with O_2 (second-order in NO concentration) in the blood is negligible compared with its reaction with Hb. Finally, inside each RBC, NO consumption by hemoglobin can be expressed by the rate equation given in Ref. 28:

$$R_{NO}=-k_{Hb}C_{NO}C_{Hb,RBC}\approx-k_{1,lu}C_{NO}, \tag{5}$$

where k_{Hb} and $k_{1,lu}$ are the rate constants and $C_{Hb,RBC}$ is the hemoglobin concentration in the red blood cell, which remains essentially constant so the reaction can be considered pseudo-first-order in NO with the reaction rate constant $k_{1,lu}=k_{Hb}C_{Hb}$.

In order to solve the resulting set of PDEs for NO concentration, we need to specify the boundary conditions. In the radial direction, one boundary condition is implied by the no-flux condition at the center

$$\frac{\partial C_{NO}}{\partial r}=0 \quad \text{at } r=0, \tag{6}$$

while far from the vessel wall we have that the NO concentration changes slowly; therefore

$$\frac{\partial C_{NO}}{\partial r}=0 \quad \text{at } r\to\infty. \tag{7}$$

In the homogeneous one-dimensional model proposed in Ref. 28, the boundary condition of Eq. (6) was justified from the expected symmetry of the radial NO concentration profile about the vessel axis, owing to the uniform NO production from the endothelium around the vessel and subsequent uniform consumption by Hb in the lumen. In our two-dimensional model, however, while NO is still produced uniformly around the vessel, its consumption in the lumen is, in general, not symmetric about the axis, owing to a random distribution of a population of RBCs that enclose Hb. In this case, the boundary condition arises, not from symmetry, but from the fact that the changes in NO concentration, at the center of the blood vessel, are virtually nonexistent due to the strong scavenging effect of NO by Hb in the RBCs,

practically depleting all of NO before it reaches the center of the vessel. The rest of the boundary conditions in the radial direction are obtained by invoking continuity of the NO concentration profile and matching the fluxes at the interfaces between the various regions. For the azimuthal direction, we use periodic boundary conditions that express continuity of both the NO concentration and NO concentration gradients in the azimuthal direction

$$C_{NO}(\theta=0)=C_{NO}(\theta=2\pi),$$
$$\frac{\partial C_{NO}}{\partial \theta}(\theta=0)=\frac{\partial C_{NO}}{\partial \theta}(\theta=2\pi). \tag{8}$$

Model Parameters and Numerical Solution

The main parameters in the model include: (1) the diffusion coefficient of NO in the abluminal region, the endothelium, and the extracellular vascular lumen (all assumed to be the same); D_{ext}, (2) the diffusion coefficient of NO inside the RBC, D_{int}; (3) the NO permeability of the RBC membrane, ($P_{RBC,est}$ or P_{lipid}); (4) the total NO production rate in the endothelium, Q_{NO}; and (5) the rate constants for NO degradation in each region, k_{ab} and k_{Hb}. The values of these parameters have been derived from experimental data reported in the literature and are summarized in Table 1. The parameters D_{ext}, $\dot{q}$, and k_{ab} have been estimated by fitting the data of Malinski *et al.*[15] to a one-dimensional model based on oblate spherical coordinates[29] (see this reference for the detailed computations). The parameters D_{int}, $P_{RBC,est}$ have been obtained from Ref. 27. Finally, the NO-hemoglobin reaction rate constant in the RBCs, k_{Hb}, has been obtained from the recent kinetic studies in Ref. 7. Other parameters used in the numerical simulations include the radius of the blood vessel, R; the thickness of the cell-depleted zone, δ; the thickness of the endothelium region producing NO, ϵ; the effective radius of the RBC, a (modeled as a sphere); the effective thickness of the RBC membrane, δ_{RBC}; and the concentration of hemoglobin inside the RBCs, $C_{Hb,RBC}$. The values of these parameters are also given in Table 1.

In order to compute a reliable numerical solution to the model equations, a finite-element-based program was developed, within the FEMLAB simulation environment. The program consists of two user-created, interconnected sublayers. The first sublayer specifies the geometry of the system and generates the various compartments, where NO is produced, transported, and consumed, for each scenario (see the section on simulation results). The relative dimensions and positions of the various regions are fixed by this layer according to the actual physical dimensions, reported in Table 1, which serve as input data provided by the user. This layer contains also a random-event generator routine, which is used to randomly place the RBCs inside the blood vessel, when they are considered in the model. This routine uses the value of the hematocrit, provided by the user, to create and position the corresponding number of RBCs inside the lumen of the blood vessel.

The second sublayer of the program is responsible for discretizing the spatial domain of the problem into a finite number of elements and implementing the boundary conditions at the various interfaces between the compartments. The spatial discretization transforms the system of PDEs in the model into a set of nonlinear algebraic equations, for which an iterative nonlinear solver that relies on Newton's method is used to obtain the solution. Because the concentration of NO in the endothelium and close vicinity is of particular interest, an adaptive meshing (variable grid spacing) technique was implemented to allow a larger number of elements near the endothelial surfaces, where the concentration gradients are expected to be steep [see Fig. 2(b) for an example of the structure of the finite-element mesh]. A finer mesh was also used in areas where the RBCs are closely spaced and in the thin RBC membrane region. The mesh size typically ranged from 10,000 elements, in areas far from the boundaries, to 200,000 elements in the vicinity of the interfaces (such as the endothelial surfaces and the RBC membrane). In each simulation run, the consistency of the numerical solution was verified by continuously refining the mesh until further increases in the number of discretization elements did not influence the results, which ensures that the solution obtained is mesh independent. Particular attention was paid to the refinement of the mesh size in the RBC membrane region due to its very thin dimensions relative to the other spatial dimensions in the problem. The mesh size in the RBC membrane region was sufficiently refined to ensure a valid mesh-independent numerical solution. Also, although the boundary condition in Eq. (7) applies to an infinite domain, it was implemented on the outermost elements of our finite mesh, typically, 2000–4000 μm from the vessel axis. Several maximum distances were used to ensure that the results did not vary appreciably with the distance where the boundary condition was applied. Finally, after each simulation run, the solution obtained was checked by verifying that it satisfies the boundary conditions.

SIMULATION RESULTS

In order to assess the relative contribution of each of the barriers for NO mass transport, we solve the above model under four different scenarios that incorporate, sequentially, each of the transport barriers. The complexity and level of detail of the model, therefore, grows as

more transport barriers are included. Initially, we simulate the base-line scenario where NO consumption by hemoglobin is assumed to take place uniformly throughout the vascular lumen (i.e., we neglect the particulate nature of the blood as well as the presence of a cell-free zone). In the second scenario, we account explicitly for the particulate nature of the blood by confining the NO-hemoglobin interaction to take place only inside a population of highly permeable RBCs. The effect of low RBC membrane permeability and cell-free zone are neglected at this stage. In the third scenario, we model the effect of adding low RBC membrane permeability. Finally, in the fourth scenario, we add the effect of the cell-free zone and simulate the full particulate model that describes NO transport and consumption in all compartments.

Homogenous Case: Scenario 1

In this case, the blood is treated as a continuum and the NO–hemoglobin interaction is assumed to take place uniformly inside the vascular lumen. The NO transport model, therefore, consists of three differential equations describing NO production, diffusion, and consumption in the endothelium, and NO diffusion and consumption in the abluminal and luminal regions. The model, in this case, is just a two-dimensional generalization of the continuum one-dimensional model proposed in Ref. 28. While it can be argued that azimuthal gradients in NO concentration are nonexistent in this case, due to the uniform production and consumption of NO in all regions, we nonetheless consider the two-dimensional representation when solving the model because the results of this scenario will serve as the basis for comparison with the other three scenarios, all of which involve azimuthal variations. It should also be noted that, since RBCs are not modeled explicitly in this scenario, the Hb concentration term, $C_{\mathrm{Hb,RBC}}$ appearing in the rate expression for NO consumption in Eq. (5) should be replaced by the concentration of Hb in the lumen, $C_{\mathrm{Hb,lumen}}$, i.e.,

$$R_{\mathrm{NO,lumen}} = -k_{\mathrm{Hb}} C_{\mathrm{NO}} C_{\mathrm{Hb,lumen}}, \tag{9}$$

where $C_{\mathrm{Hb,lumen}}$ is related to $C_{\mathrm{Hb,RBC}}$ by a factor equal to the blood hematocrit, i.e.,

$$C_{\mathrm{Hb,lumen}} = \mathrm{Hct} \times C_{\mathrm{Hb,RBC}}, \tag{10}$$

where Hct is the blood hematocrit, or the volume fraction of RBCs in a unit volume of blood. For a given value of Hct (i.e., a given number of Hb-containing RBCs), the above calculation provides the equivalent Hb concentration of a cell-free Hb solution that fills the entire luminal region. This modification of the rate expression is needed only in the homogenous scenario because it is the only scenario where the RBCs are not modeled explicitly. In the subsequent scenarios, the NO–Hb reaction is confined within the RBCs and, therefore, the consumption rate of Eq. (5) is directly applicable. The effect of the hematocrit in these scenarios is accounted for by directly adjusting the number of RBCs.

Using a physiological Hct of 45%, the homogeneous model equations were solved for several values of k_{Hb}, the rate constant of the NO reaction with oxygenated Hb. The resulting NO concentration profiles are shown in Fig. 3(a), which depicts the mean (azimuthally averaged) NO concentration as a function of the distance from the vessel axis, for four different values of k_{Hb}. The k_{Hb} values considered range from a nominal value of $10^8\ \mathrm{M}^{-1}\,\mathrm{s}^{-1}$, which is close to the NO–Hb reaction rate constant reported in Table 1, to values describing NO–Hb reactions that are tenfold ($10^7\ \mathrm{M}^{-1}\,\mathrm{s}^{-1}$), 100-fold ($10^6\ \mathrm{M}^{-1}\,\mathrm{s}^{-1}$), and 1000-fold ($10^5\ \mathrm{M}^{-1}\,\mathrm{s}^{-1}$) slower. It is clear from Fig. 3(a) that the slower the NO–Hb reaction, the higher the NO concentration. Note that since diffusional barriers (inter-RBC diffusion, transmembrane diffusion, and RBC-free zone) act to slow down the overall rate of NO consumption by RBCs, the fold reduction in k_{Hb} displayed in Fig. 3(a) mimics the effect of adding diffusional barriers to the homogeneous model. To this extent, the concentration profiles in Fig. 3(a) provide a useful grid that will allow us in the subsequent scenarios to assess the contribution of each diffusional barrier in terms of the equivalent fold reduction in k_{Hb} it produces compared to the equivalent cell-free Hb solution.

Population of RBCs: Scenario 2

Since Hb, under physiological conditions, is packaged inside RBCs, NO consumption by Hb takes place only inside RBCs, and not everywhere in the blood vessel. Therefore, the extent to which NO is ''accessible'' for scavenging by Hb is less than what is predicted from the continuum model. Furthermore, the diffusion of NO in the extracellular space between RBCs offers an additional barrier that could slow down NO uptake. To analyze these effects, we explicitly incorporate a population of RBCs into the vascular lumen compartment of our model. Since the developed model is two-dimensional, the RBCs are modeled as circles, randomly distributed throughout the lumen. The radius of each circle corresponds to the effective spherical radius of the RBC, a, (see Table 1). In this representation, the RBC circles essentially represent projections of the population of ''spherical'' RBCs onto the two-dimensional cross section of the blood vessel. Note that this two-dimensional representation of the RBC tends to underestimate the surface/volume ratio and favor the importance of the boundary layer diffusion resistance. In the luminal space outside and near the RBCs, NO transport is assumed to

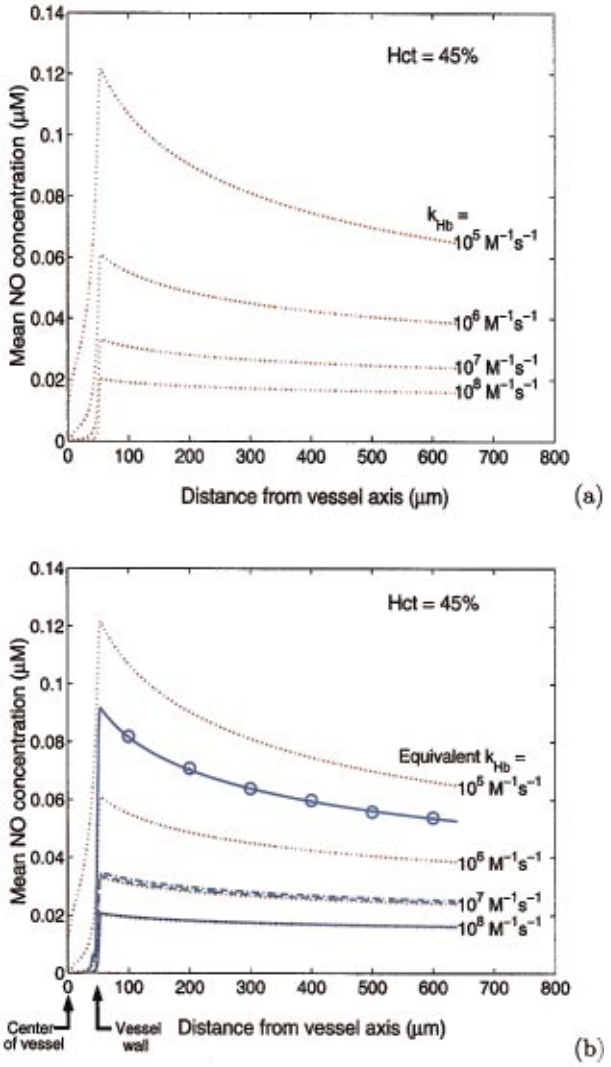

FIGURE 3. (a) **Mean NO concentration profiles, as a function of distance from the vessel axis, obtained by solving the continuum model (with 45% Hct) for $k_{Hb}=10^8$ $M^{-1}s^{-1}$, $k_{Hb}=10^7$ $M^{-1}s^{-1}$, $k_{Hb}=10^6$ $M^{-1}s^{-1}$, and $k_{Hb}=10^5$ $M^{-1}s^{-1}$. (b) Mean NO concentration profiles obtained from the continuum model ($k_{Hb}=8.9\times10^7$ $M^{-1}s^{-1}$, blue solid lines without markers), the particulate model with NO-permeable RBC membrane ($P_{mem}=\infty$, blue dashed lines), the particulate model with RBC membrane permeability of a lipid bilayer [$P_{mem}=P_{lipid}$, blue dashed-dotted lines, which almost coincides with the dashed profile ($P_{mem}=\infty$)] and the particulate model with low RBC membrane permeability ($P_{mem}=P_{RBC,est}$, blue solid line with circle markers). The dotted red profiles represent the NO concentration profiles shown in (a). 45% Hct was used in all simulations. Enclosing Hb in highly permeable RBC (dashed lines) or in RBC with lipid bilayer (dashed-dotted) results in only tenfold reduction in the NO consumption rate compared with an equivalent concentration of cell-free Hb. Under physiological Hcts, extracellular boundary layer diffusion alone cannot explain the 1000-fold reduction in NO consumption rate observed experimentally. A low transmembrane permeability (membrane and associated cytoskeleton layer) can explain the 1000-fold reduction.**

be governed only by extracellular unstirred boundary layer diffusion. The corresponding mass balance used in the extracellular space is that given in Eq. (2) with $D_{NO}=D_{ext}$ (see Table 1) and $R_{NO}=0$ (the NO reaction with O_2 in the blood is negligible compared with its reaction with Hb). For each RBC, a mass balance of the form of Eq. (2) describing the diffusion and consumption by Hb of NO inside the cell is included in the model, with $D_{NO}=D_{int}$ (see Table 1) and R_{NO} as given in Eq. (5). With this addition, the resulting NO transport model now consists of: (1) one PDE describing NO production, diffusion, and consumption in the endothelium, (2) one PDE describing NO diffusion and consumption in the abluminal region, (3) one PDE describing NO diffusion in the extracellular space between the RBCs, and (4) a population of PDEs describing the internal NO diffusion and consumption inside the population of RBCs (one PDE for each RBC). Note that, at this stage, the RBC membrane is not yet explicitly modeled and NO is assumed to diffuse freely across the membrane (i.e., $P_{mem}=\infty$). This factor will be considered in subsequent scenarios.

The number of RBCs distributed in the lumen is determined by the blood Hct, which under normal physiological conditions, is in the range of 40%–50%. In our two-dimensional model, Hct is equivalent to the fractional coverage of the luminal area by the RBC circles. For a meaningful comparison with the continuum model result, the same Hct value of 45% was used in solving the particulate model equations. The resulting mean NO concentration profile is shown by the blue dashed lines in Fig. 3(b). It should be noted here that since the RBCs are assumed to be randomly placed in the blood vessel, the NO concentration profile will depend, in general, on the particular random distribution of the RBCs, especially at low Hct where the intercellular spacing between the few RBCs present can vary significantly from one random placement to another. To eliminate this dependence on the randomness of RBC placement, the NO concentration profile is obtained by averaging the results over an exhaustive set of random RBC distributions. For large Hct values [such as the one used in Fig. 3(b)], however, the NO distribution is essentially independent of the RBC placement because of the resulting tight packing of the RBCs. This fact was verified in our simulations by solving the model equations for a large number of random RBC distributions. In all cases, only negligible variations in the NO concentration profile were observed.

Included in Fig. 3(b) also (blue solid line without markers) is the NO concentration profile obtained from the homogeneous model using the NO–Hb reaction rate constant given in Table 1. By comparing the profile of the particulate model (blue dashed) with that of the homogeneous model (blue solid) it is clear that enclosing

Hb in NO-permeable RBCs, at 45% Hct, leads to slightly less than a twofold increase in NO concentration compared to the homogeneous model. More importantly, by comparing the particulate model profile (dashed) with the ''grid'' profiles [obtained earlier in Fig. 3(a) and reproduced in Fig. 3(b) with dotted red lines for convenience of comparison], it can be seen that the particulate model (with NO-permeable RBCs) produces a concentration profile that practically coincides with the one obtained from the homogeneous model using $k_{Hb} = 10^7\ M^{-1}\,s^{-1}$. This implies that, at 45% Hct, enclosing Hb in NO-permeable RBCs in effect slows the effective NO consumption rate by no more than an order of magnitude, compared to the equivalent cell-free Hb solution. This result suggests that extracellular diffusion alone cannot explain the 1000-fold reduction in the effective NO consumption rate observed experimentally. Recall that because of our two-dimensional assumptions, the model underestimates the surface/volume ratio of the RBCs and, therefore, overestimates the boundary layer diffusion resistance. However, even under this conservative estimation, diffusion through the boundary layer is not limiting. We would expect that in the real three-dimensional case, where surface/volume ratio increases significantly, diffusion through the extracellular boundary layer would be more efficient and thus contributes even less to the overall mass transfer resistance.

Effect of RBC Transmembrane Barrier: Scenario 3

So far in our model, we have neglected the potential role of the RBC membrane in reducing NO uptake in the blood by assuming that the RBC membrane is highly permeable to NO. Based on this assumption, it has been suggested in the literature that NO consumption is limited mainly by the mass transfer resistance of the diffusion layer adjacent to the RBC membrane. Recently in Refs. 8, 26, and 27, however, combination of various experimental techniques together with model analysis have been used to show that the RBC may possess an intrinsic mechanism that can slow down NO uptake. The results of this work point to the RBC membrane and the associated cytoskeleton layer as a significant barrier to NO transport into RBC. To investigate this effect using our model, we explicitly model the RBC membrane by enclosing each cell in the population with a thin layer whose thickness corresponds to the effective thickness (based on spherical geometry) of the RBC (see Table 1). Inside these layers, NO is transported by diffusion and is not consumed by Hb. The value of the NO diffusion coefficient inside the membrane is computed directly from the RBC membrane permeability, using the film theory approximation

$$D_{mem}\frac{\partial C_{NO}}{\partial r} \approx \frac{D_{mem}}{\delta_{RBC}}(C_{NO,ext} - C_{NO,cyt}) = P_{mem}(C_{NO,ext} - C_{NO,cyt}), \qquad (11)$$

where D_{mem} is the effective NO diffusion coefficient inside the membrane (including the cytoskeleton layer), $C_{NO,ext}$ is the NO concentration at the interface between the membrane and extracellular space, $C_{NO,cyt}$ is the NO concentration at the interface between the membrane and the intracellular region (cytosol), δ_{RBC} is the thickness of the membrane, and P_{mem} is the NO permeability of the membrane. This computation is justified by the very small thickness of the membrane relative to the diameter of the RBC. Equation (11) assumes there is no solubility factor due to a hydrophilic medium (water) and a hydrophobic membrane. The analysis is still valid, however, since the D_{mem} value calculated would be the product of diffusivity and solubility (assuming the solubility is the same on both sides of the membrane).

Due to the thin dimensions of the RBCs, the finite-element mesh size was refined sufficiently in the membrane region and close vicinity to ensure a reliable numerical solution. Furthermore, similar to the previous scenario, the model was solved here, using 45% Hct, for several random RBC placements with no appreciable variations in the results. Two values for the RBC membrane permeability were considered in solving the model: (1) the membrane permeability of a lipid bilayer ($P_{mem} = P_{lipid}$; see Table 1) and (2) the low membrane permeability estimate obtained in Ref. 27 ($P_{mem} = P_{RBC,est}$; see Table 1). The resulting mean NO concentration profiles for both values are depicted in Fig. 3(b) by the blue dashed-dotted profile and the circle-marked blue solid profile, respectively. By comparing with the blue dashed profile (RBCs with completely permeable NO-membrane, i.e., $P_{mem} = \infty$), it is clear that using the lipid membrane permeability yields practically the same concentration profile, while using the low membrane permeability estimate in Ref. 27 results in nearly a threefold increase in endothelial and abluminal NO concentrations. More importantly, comparison with the red dotted ''grid'' profiles indicates that enclosing Hb in RBCs with a low transmembrane permeability, at 45% Hct, effectively slows the NO consumption rate by about 500-fold, compared to the equivalent cell-free Hb solution (effective $k_{Hb} = 2\times10^5\ M^{-1}\,s^{-1}$). This result is consistent with experimental data showing that RBCs consume NO about 600–1000 fold slower than the equivalent concentration of cell-free Hb.

Analysis of the Effect of Hct on NO Consumption Rate. One of the important factors that directly influences the level of NO consumption in the blood is the blood Hct. By definition, this factor determines the number of RBCs

present in a fixed volume of blood and, therefore, controls the extent to which NO is consumed through its interaction with Hb contained in the RBCs. This, in turn, affects how far NO travels inside the blood vessel. In scenarios 1–3, considered so far, we have used a physiological Hct (45%) to solve the model equations and, subsequently, analyze the contribution of extracellular diffusion (scenario 2) and RBC membrane permeability (scenario 3). In this section, we use our detailed model to investigate the quantitative effect of varying Hct on the NO concentration profiles and the effective NO consumption rate. To this end, we solve the model equations for several values of Hct and repeat, for each value, the same computations performed in scenarios 1–3. For the first scenario (homogeneous model), where the RBCs are not modeled explicitly, Hct is varied by adjusting the Hb concentration inside the luminal region. For scenarios 2 and 3, where the RBCs are modeled explicitly, Hct is varied by adjusting the number of RBCs in the luminal compartment of the model.

Figure 4 depicts the mean NO concentration profiles (for scenarios 1–3) obtained using Hct values of 25% (a), 15% (b), and 5% (c), respectively. Included in each plot (dotted lines) also are the corresponding ''grid'' profiles obtained by solving the homogenous model, for the given Hct, for various values of k_{Hb}. By comparing Fig. 4 with Fig. 3(b), it is clear that the NO concentration increases as Hct decreases. More importantly, the extracellular diffusion barrier (scenario 2) becomes increasingly significant as Hct decreases. At Hct=5%, the extracellular diffusion barrier decreases the effective NO consumption rate by about 600-fold, surprisingly consistent with the data from Liu *et al.*[13] using low Hct (less than 0.01%). In addition, the contribution from the membrane barrier is diminishing as Hct is decreased. This observation can also be made by comparing the how the relative ''distance'' between the mean NO concentration profiles of the three scenarios changes as a function of Hct. In particular, we see that, as Hct decreases, the distance between the profiles of scenarios 1 and 2 increases, while that between scenarios 2 and 3 decreases. Recall that the distance between two consecutive profiles is a measure of the extent to which a given transport barrier slows down the uptake of NO. For example, the distance between the profiles of scenarios 1 and 2 reflects the effect of extracellular diffusion, while the distance between the profiles of scenarios 2 and 3 reflects the effect of the low RBC membrane permeability. In light of this interpretation, the trend observed above suggests an increasingly important role for extracellular diffusion in slowing down NO uptake at low Hct. This is further confirmed by the fact that, at 5% Hct [Fig. 4(c)], extracellular diffusion alone can explain an effective NO–Hb reaction rate that is about 1000-fold smaller than the reaction rate between NO and cell-free Hb [compare the dashed and dotted profiles in Fig. 4(c)]. In contrast, at 45% Hct [Fig. 3(b)], extracellular diffusion could explain only a 10-fold reduction in the effective NO–Hb reaction rate [compare the dashed and dotted profiles in Fig. 3(b)].

We saw in scenario 3 that enclosing Hb in RBCs, at 45% Hct, with a lipid membrane permeability yields only a ten-fold reduction in k_{Hb} (compared to the equivalent cell-free Hb solution) while the low permeability estimate, $P_{\mathrm{RBC,est}}$, was able to account for about 500-fold reduction. To investigate the relationship between the RBC membrane permeability, P_{mem}, and the equivalent effective NO–Hb reaction rate constant, k_{Hb}, and how this relationship is modulated by Hct, we solved the particulate model for various values of P_{mem}, and solved the homogeneous model for various values of k_{Hb}. Then, by matching similar NO concentration profiles obtained from both models, each value of P_{mem} was assigned an equivalent k_{Hb}, which describes the effective rate of NO consumption in an equivalent concentration of cell-free Hb. The results are summarized in Fig. 5, which displays (on a log–log scale) the effective NO–Hb reaction rate constant as a function of permeability, for four different values of Hct.

For a given Hct, it is clear from the shape of the profiles in Fig. 5 that at high permeability the effective NO–Hb reaction rate constant is essentially independent of membrane permeability. In this regime, the effective k_{Hb} approaches the coefficient of the reaction rate between NO and completely NO-permeable RBCs (with $P_{\mathrm{mem}}=\infty$). In the low permeability regime, however, the reaction rate constant drops as permeability decreases. Furthermore, for a given value of membrane permeability, Fig. 5 shows that the effective reaction rate constant decreases as Hct decreases. This implies that, while a low membrane permeability is needed to explain the 1000-fold reduction in the effective NO consumption rate at high Hct, a large permeability (P_{lipid}, for example) is sufficient to explain the same fold reduction in k_{Hb} at low Hct. For example, we see that, at 45% Hct, a transmembrane permeability value less than 400 μm/s is needed to account for 1000-fold reduction in k_{Hb} from 10^8 to 10^5 $\mathrm{M}^{-1}\,\mathrm{s}^{-1}$. At 5% Hct, however, an infinite value for permeability, $P_{\mathrm{mem}}=\infty$ can explain this reduction. These findings are consistent with the fact that, at low Hct, the RBC membrane barrier contributes less to the overall transport resistance compared with extracellular diffusion, which becomes the dominant barrier.

Computation of Fractional Resistances. In this section, we use the simulation results obtained in scenarios 1–3 to quantify the contribution of extracellular diffusion and the RBC membrane barriers relative to the overall mass transfer resistance for NO. To this end, we will adopt the classical definition of transfer resistance as the ratio be-

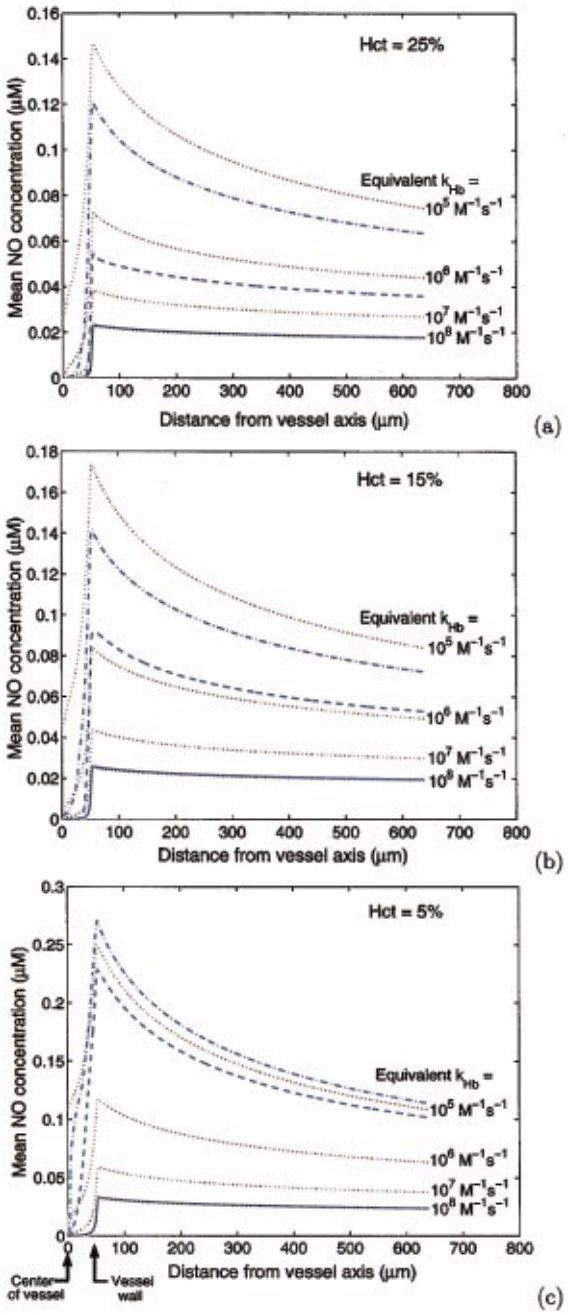

FIGURE 4. Mean NO concentration profiles, as a function of distance from the vessel axis, obtained from the continuum model ($k_{Hb}=8.9\times10^7$ $M^{-1}s^{-1}$, blue solid lines), the particulate model with NO-permeable RBC membrane ($P_{mem}=\infty$, blue dashed lines), and the particulate model with low RBC membrane permeability ($P_{mem}=P_{RBC,est}$, blue dashed-dotted lines) using (a) 25% Hct, (b) 15% Hct, and (c) 5% Hct. The red dotted profiles in each plot represent the NO concentration profiles obtained by solving the corresponding homogeneous model (with the corresponding Hct) for various values of k_{Hb}. At low Hct (5%), enclosing Hb in highly permeable RBC leads to nearly 1000-fold reduction in the equivalent NO consumption rate. Boundary layer diffusion is the key source of NO mass transport resistance at low Hct.

tween the driving force for mass transfer and the flux of the transported species. The driving force for NO transport in the blood vessel is taken to be the difference between NO concentrations at the center of the vessel ($r=0$) and at the vessel wall ($r=R$). Since the NO concentration at the vessel wall varies in the azimuthal direction (due to the randomness of the RBC distribution), we use the mean (azimuthally averaged) NO concentration at $r=R$. Also, since the flux varies across the vascular lumen both in the radial and azimuthal directions, we use a mean value by averaging over the entire area of the vascular lumen. In mathematical terms, we write

$$\text{Resistance}=\frac{\Delta C_{NO}}{N_{NO}}, \tag{12}$$

where ΔC_{NO} is the concentration difference, given by

$$\Delta C_{NO}=\overline{C}_{NO}(r=R)-C_{NO}(r=0), \tag{13}$$

where $\overline{C}_{NO}(r=R)$ is the mean NO concentration at the vessel wall, and N_{NO} is the mean flux of NO into the vascular lumen, given by

$$N_{NO}=\frac{1}{\pi R^2}\int_{\theta=0}^{\theta=2\pi}\int_{r=0}^{r=R}(-D_{NO}\nabla C_{NO})r\,dr\,d\theta. \tag{14}$$

The above double integral is computed numerically from the NO concentration data obtained by solving the model equations corresponding to each scenario. Note that in scenarios 2 and 3, the value of D_{NO} in Eq. (14) is not the same everywhere in the lumen due to the presence of different compartments (the extracellular space, the RBC membrane, and the intracellular spaces). In these cases, the mean flux is computed by partitioning the above integral into a number of subintegrals, each of which corresponds to a particular compartment, and then summing them all up. Note also that since NO concentration is essentially zero at the center of the blood vessel in all scenarios, the magnitude of the mass transfer resistance is directly proportional to the NO peak concentration at the vessel wall.

Using Eqs. (12)–(14), we initially compute the resistance associated with each of the three scenarios considered so far, with scenario 1 (homogenous model) representing the base-line resistance, created by diffusion resistance in the homogeneous phase, and scenario 3 (full particulate model) representing the total resistance. Then, by subtracting the resistance of a given scenario from the resistance of the next one, the contribution of the corresponding transport barrier can be quantified. For example, by subtracting the resistance obtained for

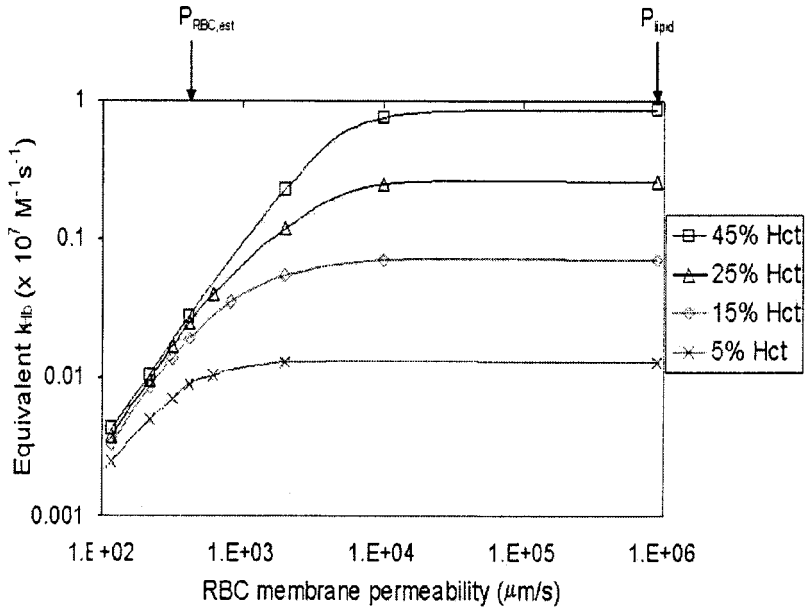

FIGURE 5. Log–log plot of the effective NO-Hb reaction rate constant, k_{Hb}, as a function of NO permeability of the RBC membrane, P_{mem}, at 45% Hct (square markers), 25% Hct (triangle markers), 15% Hct (diamond markers), and 5% Hct (cross markers).

scenario 1 from that obtained for scenario 2, we obtain the mass transfer resistance due to the packaging of Hb inside a population of NO-permeable RBCs (extracellular boundary layer diffusion). Similarly, by subtracting the resistance obtained for scenario 2 from that obtained for scenario 3, we obtain the mass transfer resistance due to the low permeability RBC membrane.

The results of the above calculations are summarized in the charts depicted in Fig. 6, which display the fractional resistance associated with each barrier as a function of Hct. Here, the fractional resistance of a given barrier is defined as the ratio of the resistance contributed by that barrier to the total resistance of all the barriers combined at the same Hct (note that by this definition, for a given Hct, the sum of the fractional resistances contributed by the different barriers must add up to 1). The results indicate that as Hct is decreased from 45% to 5%, the contribution of the RBC membrane barrier drops from 75% to about 30% while the extracellular boundary layer diffusion resistance jumps from less than 5% to about 65%. These findings are consistent with the experimental data shown in Ref. 8.

Effect of Cell-Free Zone: Scenario 4

In the particulate model scenarios 2 and 3 discussed above, the RBCs were assumed to be randomly distributed throughout the vascular lumen and were, therefore, allowed to get arbitrarily close to the vessel wall. Under flow conditions, however, and due to the hydrodynamic effects of blood flow, the RBCs tend to migrate towards the center of the vessel, thus creating a cell-depleted zone, or layer, near the vascular wall where NO has to travel across before it reaches Hb inside the RBCs. The effect of this layer has been verified experimentally.[12] Intuitively, since NO is not consumed by Hb in this region, the cell-free layer provides an additional source for mass transfer resistance that contributes to diminishing the NO-scavenging effect of the blood. To account for this effect, we add a thin RBC-free layer near the vascular wall in our particulate model. The entire RBC population is therefore confined to a smaller region in the luminal compartment. The thickness of the RBC-free layer depends on fluid mechanical considerations. In our simulations, the thickness of the cell-free zone was taken to be 2.5 μm.[20] The resulting NO concentration profiles, for 45% Hct, are shown in Fig. 7 by the square-marked blue solid lines (using $P_{mem}=\infty$) and the diamond-marked blue solid lines (using $P_{mem}=P_{RBC,est}$). In both cases, it is clear that NO concentration increases relative to the corresponding model with no cell-free zone. Also, by comparing these profiles against the ''grid'' profiles (red dotted lines), it is clear that the addition of the RBC-free zone to a population of NO-permeable RBCs in effect reduces the NO consumption rate by about 50-fold while the addition of the RBC-free zone to a population of RBCs with low membrane permeability results in more than 800-fold reduction. The two-dimensional NO distribution in all of the model compartments is shown in Fig. 8.

DISCUSSION

It is commonly observed that RBC consumes NO at a rate about 600–1000 times slower than the equivalent concentration of cell-free Hb.[3,8,12,13,26] Whether NO consumption by RBC is limited by an unstirred boundary layer outside of RBC, or diffusion barrier caused by the

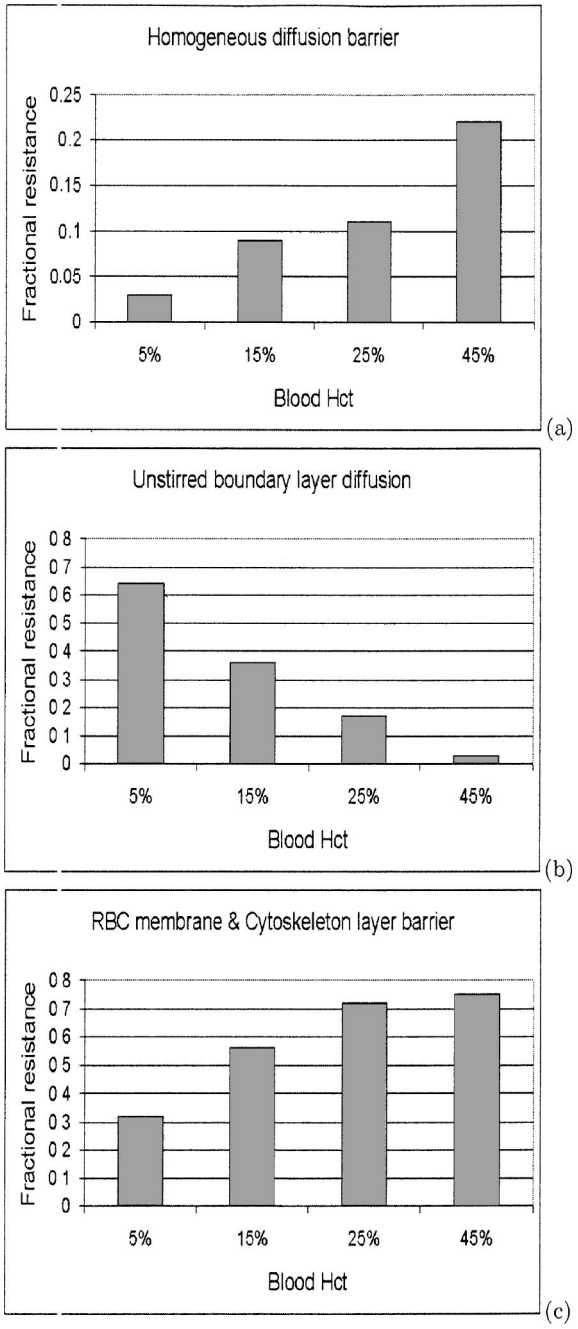

FIGURE 6. Fractional resistance (to NO uptake in the blood) associated with (a) diffusion in the homogeneous phase, (b) unstirred boundary layer diffusion, and (c) RBC transmembrane permeability (including cytoskeleton layer), as function of Hct. The fractional resistance of each barrier is defined as the ratio of the resistance contributed by that barrier to the total resistance of all the barriers combined at the same Hct. At 45% Hct, more than 70% of the total resistance is contributed by the RBC membrane and cytoskeleton layer, while less than 5% is contributed by extracellular (unstirred layer) diffusion in the vicinity of the RBCs. At 5% Hct, close to 65% of the total resistance is contributed by diffusion in the unstirred boundary layer while about 30% is contributed by the RBC membrane and cytoskeleton layer.

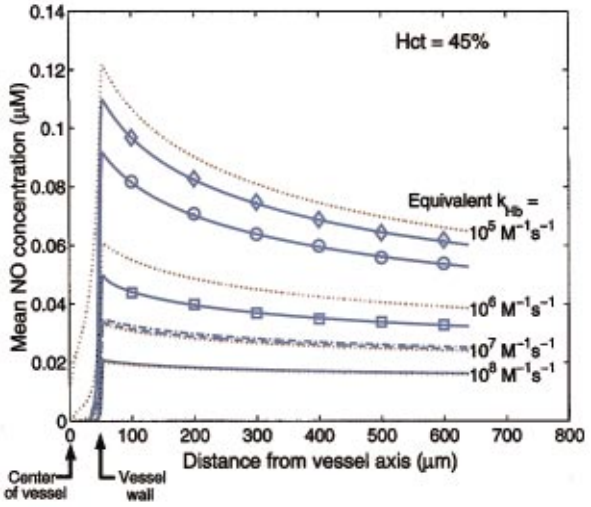

FIGURE 7. Mean NO concentration profiles obtained from the continuum model ($k_{Hb}=8.9\times10^7$ $M^{-1}s^{-1}$, blue solid lines), the particulate model with NO-permeable RBC membrane ($P_{mem}=\infty$, blue dashed lines), the particulate model with RBC membrane permeability of a lipid bilayer ($P_{mem}=P_{lipid}$, blue dashed-dotted lines, which coincide with the blue dashed profile), the particulate model with $P_{mem}=\infty$ and RBC-free zone (blue solid lines with square markers), the particulate model with low RBC membrane permeability and no RBC-free zone ($P_{mem}=P_{RBC,est}$, blue solid lines with circle markers), and the particulate model with $P_{mem}=P_{RBC,est}$ and RBC-free zone (blue solid lines with diamond markers). The red dotted profiles represent the NO concentration profiles obtained by solving the continuum model for various values of k_{Hb}. In all simulations, 45% Hct was used.

membrane and associated cytoskeleton is an on-going subject of research.[8,13,14,23,26] Previous studies using either extremely low Hct ($<0.01\%$),[13] or near physiological Hct ($5\%-15\%$),[8,26] yielded different conclusions. Since experiment under high Hct conditions is relatively difficult, and since diffusion reaction is a well-characterized physical chemical process, mathematical modeling using experimentally derived parameters is a powerful tool to gain insight. Here, we presented a model which accounts explicitly for the effects of inter-RBC diffusion of NO and diffusion barrier caused by RBC membrane and associated cytoskeleton.

Using the experimentally derived parameters, we calculated the NO concentration profiles under various Hcts and conducted various ''in silico'' experiments. Our model analysis shows that under physiological conditions (Hct $=45\%$), the diffusion barrier created by the boundary layer is insignificant and insufficient to account for the 600–1000-fold reduction in the NO consumption rate. It should be noted here that the fact that this result was obtained using a two-dimensional, cylindrical representation for the RBCs lends greater support to this conclusion. The reason is that the two-dimensional (cylindrical) representation inherently underestimates the

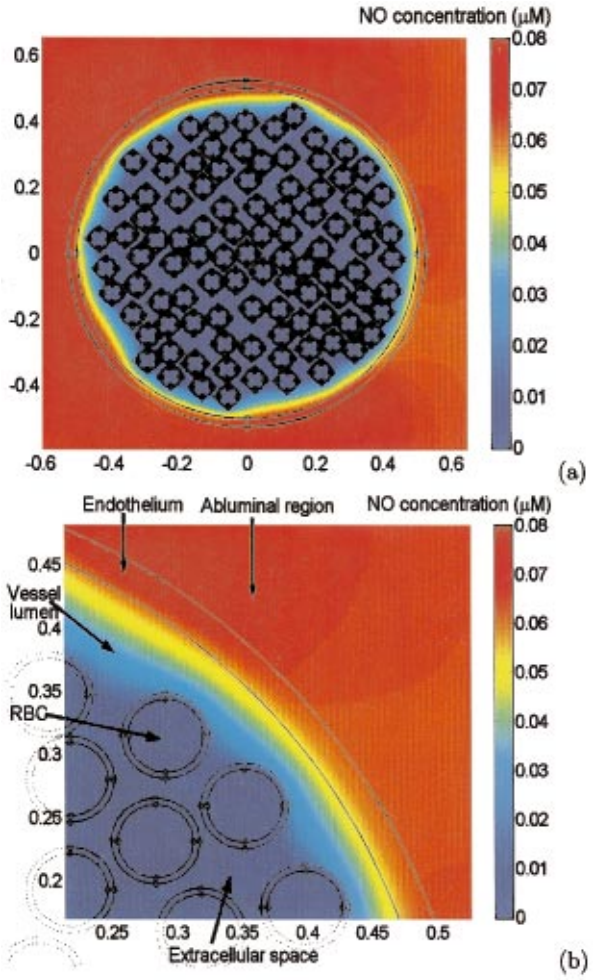

FIGURE 8. (a) Distribution of NO in all of the model compartments, including the abluminal region, the endothelium, the cell-free zone, the extracellular space in the vascular lumen, the RBC membranes and the intracellular space inside the population of RBCs, for blood Hct of 45%, and (b) a magnified view of a portion of the blood vessel (bottom plot).

diffusion speed across the extracellular boundary layer relative to the real three-dimensional (3D) (spherical) case. This point is illustrated by the difference between the Nusselt number for a cylinder and that for a sphere. In the case of a sphere suspended in an infinite medium, for example, the low Reynolds number asymptote for mass transfer is 2.0. The best (experimental) estimate of the analogous Nusselt number for the cylinder is much smaller than this (e.g., about 0.3 for the analogous heat transfer problem). From its definition, the Nusselt number is directly proportional to the external mass transfer rate and is therefore inversely proportional to the external mass transfer resistance. The smaller Nusselt number for a cylinder, therefore, signifies a smaller mass transfer rate across the boundary layer and, therefore, a larger diffusion resistance in the layer. Note that the Nusselt number, which is a dimensionless quantity, already takes into account the difference in geometry between the two representations. Related to this difference in geometry is the fact that the cylindrical representation leads to a smaller surface/volume ratio than in the spherical case, which also leads to slower diffusion rates and, hence, larger resistance. These conditions would only favor the importance of the boundary layer diffusion resistance. However, even under such conservative assumptions in favor of the boundary layer diffusion barrier, the model results show that extracellular diffusion in the boundary layer was not limiting under physiological conditions. Therefore, one would expect that when the real three-dimensional, spherical representation of the RBCs is considered (where both the Nusselt number and the surface/volume ratio are significantly higher), diffusion through the extracellular boundary layer would be more efficient and thus contributes even less to the overall mass transfer resistance.

Incorporating the membrane and cytoskeleton-associated resistance can explain the large difference between the NO consumption rates by RBC and cell-free Hb. The difference between RBC and cell-free Hb under high Hct condition was supported by experimental data shown in Fig. 3 of Liao *et al.*,[12] where 50% Hct of RBC (equivalent to 11 mM cell-free Hb, heme basis) in the lumen of an isolated microvessel produced less vessel constriction than 10 mM of cell-free Hb. In this experiment, RBC suspension was stationary in the lumen and thus cell-free zone did not develop. Therefore, the difference must be explained in terms of boundary layer diffusion barrier[13,14] or membrane and cytoskeleton associated diffusion barrier.[8,26] Our model analysis here shows that the difference cannot be explained by extracellular boundary layer diffusion resistance and is best accounted for by the membrane and cytoskeleton-associated diffusion resistance. It should be noted that the intra-RBC diffusion limitation was conclusively ruled out by either oxidizing the intracellular Hb to metHb,[13] or depleting the intracellular Hb concentration in RBC ghosts.[8] On the other hand, extracellular boundary layer diffusion barrier was dominating under low Hct ($<5\%$) conditions. Under these conditions, the effect of membrane associated resistance becomes negligible.

The conclusions presented here contradict previous studies on NO and O_2 transport into RBCs. Previous studies[13,14,17,24,25] mainly used extremely low Hct ($<1\%$), and thus the diffusion barrier was the only conclusion, and the membrane or cytoskeleton-associated resistance could not be detected. One study using packed RBC film to evaluate effect of membrane resistance to O_2 transport from one side of the film to another[6] concluded that membrane resistance was insignificant. Under this condition, however, the O_2 transfer rate was dominated by the O_2 release rate of Hb. Thus, membrane-

associated resistance could not be accounted for. More studies are needed to completely resolve the discrepancy between various theories.

Perhaps the best support of membrane and cytoskeleton-associated resistance is by chemical modification of RBC membrane and/or cytoskeleton. Huang *et al.*[8] provided several experimental examples where RBCs are pretreated with protein cross linkers, azide, and high concentrations of NO. In these cases, the chemicals were washed away after treatment and no size and shape changes on RBC were observed. Yet, the NO consumption rate by the treated RBCs were increased or decreased, depending on the specific treatment. All the biological complications such as potential perturbations to free radical generation and metabolism have been carefully controlled (unpublished data). Moreover, the NO consumption rates were measured by both the competition experiments and an isolated vessel bioassay, which generated consistent data. Since these pretreatments did not alter the boundary layer barrier, they provided strong support for the membrane and cytoskeleton-associated barrier.

Liu *et al.*[14] recently rederived a mathematical model published by Vaughn *et al.*[26] to analyze the competition experiment.[26] They argued that extracellular diffusion is the primary limiting factor in NO consumption by RBC, contrary to the conclusion of Vaughn *et al.* Their main argument is that increasing Hct in fact makes the NO concentration ''more inhomogeneous.'' Unfortunately, this argument is based on an incorrect model, which does not account for the NO donor concentration correctly in the competition experiment. In order to keep the total amount of NO released constant, the NO donor concentration in the competition experiment is based on the *total volume*, not *the extracellular volume.*[26] Thus, when Hct increases, the donor concentration based on the extracellular volume increases as well, but the total amount of NO donor added remains constant. This was not taken into account in their calculation. As such, Eq. (13) and the following equations in Liu *et al.*,[14] incorrectly assumed the extracellular NO donor concentration is constant as Hct increases. Therefore, when Liu *et al.*[14] increased Hct, the total amount of NO released decreased, and of course the NO flux into RBC decreased as well. After correcting for the extracellular volume change when varying Hct, the flux monotonically increases as Hct increases. Here, we show that increasing Hct decreases the particulate behavior and decreases extracellular boundary layer. This phenomenon can be intuitively reasoned using a limiting case of infinitely small Hct. Under this condition, extracellular diffusion has the largest contribution, contrary to the claim of Liu *et al.*[14]

The cause of the surprisingly low permeability of RBC membrane is not completely understood. Our tentative model is based on the cytoskeleton and associated NO-inert proteins.[8] It has been shown that RBC cytoskeleton is a net of spectrins anchored indirectly to band 3.[21,22] Although the measured spectrin network is too loose to account for the 600-1000 fold reduction in NO permeability, it is possible that the cytoskeleton network was loosened during sample preparation. In addition, this layer of cytoskeleton is known to bind to various NO-inert proteins, such as metHb and Heinz bodies. The combination of spectrin and these associated NO-inert proteins forms a 3D tortuous mesh of cytoskeleton, which reduces the gas transport rate. This model, although partially supported by data in Huang *et al.*,[8] remains to be refined as more data are available.

Another theory to explain the NO bioavailability centers on the formation of S-nitroso-Hb.[10,16] This theory requires *R* to *T* transition of Hb and is mainly designed to explain the long-range delivery of NO from the lung to the tissue. Here, we are addressing the local effect of NO production by endothelial cells and consumption by RBCs, particularly in arteries and arterioles. Under this local condition, the *R* to *T* transition of Hb does not occur. Thus, the S-nitroso-Hb formation was not explicitly considered. The formation of S-nitroso-Hb does not affect local vessel regulation as it would be delivered to oxygen depleted tissue at a distance.[16]

ACKNOWLEDGMENT

Financial support, in part by the National Science Foundation and the National Institutes of Health, is gratefully acknowledged.

REFERENCES

[1] Buerk, D. G. Can we model nitric oxide biotransport? A survey of mathematical models for a simple diatomic molecule with surprisingly complex biological activities. *Annu. Rev. Biomed. Eng.* 3:109–143, 2001.

[2] Butler, A. R., I. L. Megson, and P. G. Wright. Diffusion of nitric oxide and scavenging by the blood in the vasculature. *Biochim. Biophys. Acta* 1425:168–176, 1998.

[3] Carlsen, E., and J. H. Comroe, Jr. The rate of uptake of carbon monoxide and of nitric oxide by normal human erythrocytes and experimentally produced spherocytes. *J. Gen. Physiol.* 42:83–107, 1958.

[4] Cassoly, R., and Q. H. Gibson. Conformation, cooperativity, and ligand binding in human hemoglobin. *J. Mol. Biol.* 91:3301–3313, 1974.

[5] Eich, R. F., T. S. Li, D. D. Lemon, D. H. Doherty, S. R. Curry, J. F. Aitken, A. J. Mathews, K. A. Johnson, R. D. Smith, G. N. Phillips, and J. S. Olson. Mechanism of NO-induced oxidation of myoglobin and hemoglobin. *Biochemistry* 35:6976–6983, 1996.

[6] Kutchai, H., and N. C. Staub. Steady-state, hemoglobin-facilitated O_2 transport in human erythrocytes. *J. Gen. Physiol.* 53:576–589, 1969.

[7] Herold, S., M. Exner, and T. Nauser. Kinetic and mechanistic studies of the NO*-mediated oxidation of oxymyoglobin and oxyhemoglobin. *Biochemistry* 40:3385–3395, 2001.

[8] Huang, K., T. H. Han, D. R. Hyduke, M. W. Vaughn, H. V. Herle, T. W. Hein, C. Zhang, L. Kuo, and J. C. Liao. Modulation of nitric oxide bioavailability by erythrocytes. *Proc. Natl. Acad. Sci. U.S.A.* 98:11771–11776, 2001.
[9] L. J. Ignarro, Nitric Oxide: Biology and Pathobiology. CA: Academic, San Diego, 2000.
[10] Jia, L., C. Bonaventura, J. Bonaventura, and J. S. Stamler. S-nitrosolhaemoglobin: A dynamic activity of blood involved in vascular control. *Nature (London)* 380:221–226, 1996.
[11] Lancaster, J. A tutorial on the diffusivity and reactivity of free nitric oxide. *Nitric Oxide* 1:18–30, 1997.
[12] Liao, J. C., T. W. Hein, M. W. Vaughn, K. Huang, and L. Kuo. Intravascular flow decreases erythrocyte consumption of nitric oxide. *Proc. Natl. Acad. Sci. U.S.A.* 96:8757–8761, 1999.
[13] Liu, X., M. J. S. Miller, M. S. Joshi, H. Sadowska-Krowicka, D. A. Clark, and J. R. Lancaster. Diffusion-limited reaction of free nitric oxide with erythrocytes. *J. Biol. Chem.* 273:18709–18713, 1998.
[14] Liu, X. P., A. Samouilov, J. R. Lancaster, and J. L. Zweier. Nitric oxide uptake by erythrocytes is primarily limited by extracellular diffusion not membrane resistance. *J. Biol. Chem.* 277:26194–26199, 2002.
[15] Malinski, T., Z. Taha, S. Grunfeld, S. Patton, M. Kapturczak, and P. Tomboulian. Diffusion of nitric oxide in the aorta wall monitored *in situ* by porphyrinic microsensors. *Biochem. Biophys. Res. Commun.* 193:1076–1082, 1993.
[16] McMahon, T. J., R. E. Moon, B. P. Luschinger, M. S. Carraway, A. E. Stone, B. W. Stolp, A. J. Gow, J. R. Pawloski, P. Watke, D. J. Singel, C. A. Piantadosi, and J. S. Stamler. Nitric oxide in the human respiratory cycle. *Nat. Med.* 8: 711–717 (2002).
[17] Merchuk, J. C., Z. Tzure, and N. Lightfoot. Diffusional resistances to oxygen transfer in whole blood. *Chem. Eng. Sci.* 38:1315–1321, 1983.
[18] Pohl, U., and D. Lamontagne. Impaired tissue perfusion after inhibition of endothelium-derived nitric oxide. *Basic Res. Cardiol.* 86:97–105, 1991.
[19] Rice, S. A. Hydrodynamic and diffusion considerations of rapid-mix experiments with red blood cells. *Biophys. J.* 29:65–78, 1980.
[20] Schmidt-Schönbein, H., T. Fisher, G. Driessen, and H. Rieger. In: Microcirculation. Baltimore, MD: University Park Press, 1979, pp. 353–418.
[21] Swihart, A. H., J. M. Mikrut, J. B. Ketterson, and R. C. Macdonald. Atomic force microscopy of the erythrocyte membrane skeleton. *J. Microsc.* 204:212–225, 2001.
[22] Takeuchi, M., H. Miyamoto, Y. Sako, H. Komizu, and A. Kusumi. Structure of the erythrocyte membrane skeleton as observed by atomic force microscopy. *Biophys. J.* 74:2171–2183, 1998.
[23] Tsoukias, N. M., and A. S. Popel. Erythrocyte consumption of nitric oxide in presence and absence of plasma-based hemoglobin. *Am. J. Physiol.* 282:H2265–H2277, 2002.
[24] Vandegriff, K. D., and J. S. Olson. The kinetics of O_2 release by human red blood cells in the presence of external sodium dithionite. *J. Biol. Chem.* 259:12609–12618, 1984.
[25] Vandegriff, K. D., and J. S. Olson. Morphological and physiological factors affecting oxygen uptake and release by red blood cells. *J. Biol. Chem.* 259:12619–12627, 1984.
[26] Vaughn, M. W., K. T. Huang, L. Kuo, and J. C. Liao. Erythrocytes possess an intrinsic barrier to nitric oxide consumption. *J. Biol. Chem.* 275:2342–2348, 2000.
[27] Vaughn, M. W., K. T. Huang, L. Kuo, and J. C. Liao. Erythrocytes consumption of nitric oxide: Competition experiment and model analysis. *Nitric Oxide* 5:18–31, 2001.
[28] Vaughn, M. W., L. Kuo, and J. C. Liao. Effective diffusion distance of nitric oxide in the micocirculation. *Am. J. Physiol.* 43:H1705–H1714, 1998.
[29] Vaughn, M. W., L. Kuo, and J. C. Liao. Estimation of nitric oxide production and reaction rates in tissue using a mathematical model. *Am. J. Physiol.* 43:H2163–H2176, 1998.